Originally published 23 July 2015; corrected 9 October 2015.

www.sciencemag.org/cgi/content/full/science.aac4315/DC1

Supplementary Materials for

Abrupt warming events drove Late Pleistocene Holarctic megafaunal turnover

Alan Cooper,* Chris Turney,* Konrad A. Hughen,
Barry W. Brook, H. Gregory McDonald, Corey J. A. Bradshaw

*Corresponding author. E-mail: alan.cooper@adelaide.edu.au (A.C.);
c.turney@unsw.edu.au (C.T.)

Published 23 July 2015 on *Science* Express
DOI: 10.1126/science.aac4315

This PDF file includes:

Other Supplementary Material for this manuscript includes the following:
(available at www.sciencemag.org/cgi/content/full/science.aac4315/DC1)

Tables S1 and S4 as Excel files

Correction: An old version of Table S4 was inadvertently submitted. It was been replaced with the correct, updated version.

Materials and Methods, and Supplementary Text

Dating megafaunal events

GRIWM analyses of megafaunal radiocarbon dating series

Confirming the presence of a species in a given area becomes increasingly difficult as it declines to low densities, such that estimating the exact extinction time is virtually impossible (35, 43). This problem is exacerbated in the macrofossil record because of the typical scarcity of data, uncertainty in radiometric dating, variable sampling rates, and changing conditions for fossil preservation and taphonomy. Thus, the laboratory sample uncertainty associated with the youngest radiometrically dated specimen in a fossil time series is unlikely to encompass the true extinction date, unless the sampling intensity is particularly high or the underlying reduction in the population's density is abrupt (35, 43). Various statistical methods have been developed to estimate extinction times from a time series of records, both with and without associated dating uncertainty. A recent innovation, the 'Gaussian-Resampled Inverse-Weighted McInerney' (GRIWM) method, has been shown to exhibit strong performance on a range of simulated data (35, 43). We applied GRIWM to the calibrated radiocarbon data to estimate the unobserved temporal range for all the dated time series, which would be beyond the terminal observation (i.e., beyond the youngest date for extinction events, or oldest date for invasion events).

GRIWM necessarily estimates wider confidence intervals for the terminal estimate than calibrated terminal AMS dates because it also incorporates the uncertainty in the sampling distribution of all the dated specimens (i.e., not just the estimated age uncertainty of the terminal specimen). For this reason, and because there is a lack of information about the form of the underlying population density reduction (extinctions) or increase (invasions), we also analysed all climate randomisations using the terminal OxCal Phase-calibrated AMS date in each series only (see below).

Megafaunal data series – radiocarbon (14C) calibration

For the megafauna samples, radiocarbon ages younger than 12,500 ^{14}C years were calibrated using the dendro-dated part of IntCal13 *(36)*. For ages > 12,500 ^{14}C years, recent work has demonstrated the potential for divergence between palaeo-archives and either Greenland ice core chronologies or IntCal timescales, especially at the older part of the radiocarbon timescale *(23).* As described in Section 3 below, we circumvent this problem through the use of the Cariaco Basin marine sediment record, which contains both a detailed climate chronology tuned to the calendar age Hulu Cave timescale (*44*), and a comprehensive radiocarbon series *(28)*, critically allowing direct comparison between radiocarbon ages and climate (Fig. S2, S4). The use of the existing Cariaco Basin record for calibration of ages older than 12,500 ^{14}C years allows us to use our new combined chronology to date both climate and megafaunal events, prior to correlation tests. Although a marine record, Cariaco Basin preserves a remarkably detailed record of atmospheric ^{14}C. Importantly, although the ^{14}C marine offset appears to disappear during Heinrich 1 and the very onset of the YD stadial, there is no evidence for changes in reservoir age at other times, or during interstadials *(44)*.

In addition to the individual age calibrations, we applied the *Phase* function, a Bayesian dating model, of OxCal *(34, 45)* to improve the precision on the error bounds for the terminal age in each data series, either the youngest (for extinctions) or oldest (for invasions). Phases are a defined set of ages (e.g., a data series of

radiocarbon dates) and are bounded, where it is assumed that ages within the boundaries are sampled from a uniform distribution. For extensive data series such as the Eurasian mammoths, North American mammoths, and Russian woolly rhino, the *Phase* calibration could not be performed on the entire dataset, so the last 200, 150 and 150 dates, respectively, were used. The *Phase*-calibrated terminal ages (not the *Phase* boundaries) were tested for correlations with climate events recorded in the GICC05, and the Cariaco-Greenland timescales, in parallel with the values from the GRIWM estimates of the potential unobserved temporal range of each taxon. The *Phase*-calibrated terminal ages were included to provide a conservative approach where only the observed, rather than predicted (as in GRIWM), data were used in randomization tests.

Megafaunal data series

Megafaunal taxa with extensive, well-controlled series of AMS radiocarbon-dated bones and/or ancient DNA data were examined for evidence of major megafaunal transitions, e.g., where a major clade or entire species becomes globally extinct or regionally extirpated (designated *extinction*), or appears for the first time in a region (designated *invasion*). Events without genetic data, but where the fossil record clearly details global or regional extinction events, were also recorded as megafaunal transition events (e.g., *Palaeoloxodon* in Japan, *Equus francisci* in Alaska, or many of the terminal Pleistocene events in the New World, Table S1, S2, Fig. 1). Observations were combined across broad biogeographic areas, e.g., Europe, eastern Beringia (Alaska and Yukon), North America (south of Late Pleistocene Laurentide Ice Sheets) to maximize the chances that the transition events detected represent widespread regional events, and minimize the chances of taphonomic biases. However, where high-quality local fossil series existed these were also used, e.g., *Palaeoloxodon* in Japan, *Coelodonta* in Britain and Wrangel Island, and Neandertals across Europe *(46)*, where the records were sufficient (Table S1, S2).

We have attempted to analyze mostly AMS radiocarbon dates generated after the year 2000 (ideally where large molecular weight proteins extracted using ultrafiltration were dated) to minimize the risk of contamination during gelatization, especially at the older end of the radiocarbon timescale using standard methods *(47, 48)* and where the error uncertainty was < 3.5%. For example, this is why we did not use the AMS data series of eastern Beringian stilt-legged horses (*Equus francisci*) *(49)* in randomization tests, because the dating analyses for these samples did not use the ultra-filtration pre-treatment method, and the error margins were too large to calibrate precisely.

Several data series were rejected due to imprecise terminal ages (e.g., Neandertal populations in different geographic subregions of Europe) or terminal ages that were clear outliers from the rest of the series (e.g., certain New World terminal Pleistocene megafauna). For example, the late survival of *Megaloceros* in the Urals is not suitable, as the precise extinction date is difficult to gauge from the small number of available dates *(39)*. In contrast, the extinction of the Western European population of *Megaloceros* is relatively well characterized *(39)*. Data series with either inadequate numbers or quality of dated specimens (e.g., New World terminal Pleistocene megafauna such as *Cervalces, Dasypus, Camelops, Bootherium, Nothrotheriops, Platygonus, Oreamnos, Castor, Megalonyx*) were excluded, as were GRIWM estimates with 95% confidence intervals larger than 5,000 years, which were identified as clear outliers (Fig. S1), vastly exceeding the mean interval of interstadials (median interstadial duration = 700 years; range: 100–2600 years) and/or stadials (1121; range: 278-8839), thus undermining the statistical power of the randomization tests. In two of these cases (*Ovibos, Coelodonta* Wrangel Island) the confidence interval for the terminal AMS date was still sufficiently narrow that it could be used in the randomization tests (Table S1, S2). Given the old age of the

Ovibos date, we tested whether the presence of the larger error margin impacted the power of the randomization tests as a separate variable (Table 1, Figure 2). Apart from these exceptions, we have included all species for which suitable data exist.

It is possible that the fossil deposition rate might decrease in association with climatic events, or some other factor, thereby confounding our ability to date megafaunal transitions accurately. However, in four cases the extinction of one species or clade in an area was rapidly followed by the replacement by a conspecific or congeneric (e.g., *Bison priscus*/*Bison x* in Europe or *Arctodus* and *Ursus arctos* in eastern Beringia) or another clade (e.g., *Ursus spelaeus* in Germany, *Mammuthus primigenius* in Europe), strongly arguing against taphonomic artefacts associated with fossil preservation controlling the patterns observed. Furthermore, the broader record of mammoth (*Mammuthus primigenius*) fossils in Eurasia and the New World (Table S1) *(50)* is plotted on Fig. 1 to demonstrate the lack of any large-scale hiatus in fossil deposition, especially during the time periods of interest (e.g., post-glacial New World). It is worth noting that mammoths are thought to have been absent from Europe for short periods (e.g. 19-21 kyr) *(39)*. The latter study analysed temporal range shifts and the concentration of specimens to suggest that humans initially had little impact on megafaunal populations such as the mammoth in Eurasia and elsewhere, until population fragmentation due to climate changes in the terminal Pleistocene. Similarly, although Fig. 1 records the initial presence of anatomically modern humans (AMH) in Europe around 44-45 kyr *(2, 46)*, there is little evidence that the small pre-Glacial populations were involved in the regional extirpation events of Eurasian megafauna *(50)*.

The absence of megafaunal population studies using ancient nuclear DNA data meant that all genetic datasets were of mitochondrial loci, usually the hypervariable segments of the control region, which are commonly used for population genetics analyses. Mitochondrial genes are maternally inherited in vertebrates, so the genetic transitions analysed here represent an interruption of continuous female lineages, whether by extinction, replacement or genetic drift. In many of the replacement events, the large diversity on either side of the genetic transition, and/or the rapid pace of the transition itself, would argue against genetic drift as a principal driver.

The maternal inheritance of mitochondrial genes has the effect of reducing the effective population size, increasing the sensitivity to population bottlenecks compared to single nuclear loci. As a result, the single locus mitochondrial data have a limited ability to resolve complex palaeodemographic events compared to multiple nuclear loci. Analyses suggest that Bayesian coalescent analyses (e.g., skyline and skyride plots) of large diverse mtDNA populations through time might have limited ability to detect rapid or shallow bottlenecks *(21)*. Indeed, in large diverse populations it is possible that rapid shifts might not be easily detected by these models if precursor and replacement populations include overlapping genetic diversity. Together this might explain the apparent contrast between the abrupt shifts identified here and generic longer longer-term population trends inferred in previous megafaunal paleodemographic analyses of ancient mtDNA *(9, 13)*.

Developing a highly-resolved time scale of climate change

While it is possible to simply compare the timing of the megafaunal events with Greenland ice records using the GICC05 timescale, recent work has identified a major offset in the calendar ages obtained from the international standard radiocarbon calibration curve IntCal13 and the GICC05 record *(23, 24)*. In order to

place the timing of megafaunal transitions directly onto records of late Pleistocene climate change, such as GICC05, we first explored differences in calibrated ages generated from IntCal13 *(36)* with an alternative detailed record of radiocarbon dates: the marine Cariaco Basin radiocarbon sequence obtained off the north coast of Venezuela *(28, 33)*. While the Cariaco Basin sequence forms a significant part of the IntCal13 curve, the latter is generated using a random walk model that takes into account the additional uncertainties and error structures of other contributing datasets *(36)*, potentially resulting in different calendar ages. To examine the relationship, we calibrated a suite of 355 radiocarbon dated Eurasian mammoths >12,500 ^{14}C years (kyr BP). We observe multi-centennial differences in mean age throughout the range of the dating method, typically longer than the duration of interstadials recorded in the North Atlantic *(16)* (Fig. S2). In addition, IntCal13 reaches the limit of resolution around 45 thousand calendar years (kyr), limiting the time range possible for examination.

Cariaco Basin provides an additional important benefit over direct calibration using IntCal13 as the Cariaco sequence also preserves a sensitive measure of climate change, recording interstadial shifts in the trade winds associated with the Intertropical Convergence Zone (ITCZ) in the tropical Atlantic *(28)*, apparently driven by changes in the hemispheric temperature gradient *(37)*. The Cariaco Basin sediments are laminated annually during the Late-glacial and Holocene, providing independent age control back to 14.7 kyr. Prior to 14.7 kyr, the sedimentary record preserves evidence of distinct millennial-scale variability in sedimentological and geochemical records that have been robustly correlated along the ITCZ with changes in the East Asian Monsoon intensity preserved in the uranium-series dated Hulu Cave record in China *(44)*, placing the sequence on a calendar age timescale *(28, 33)*. Cariaco Basin therefore provides a valuable means of directly correlating radiocarbon dates with a climate record, allowing fine-scale comparison of the megafaunal extinction ages with climatic events *(41)*.

To investigate whether changes in the ITCZ associated with interstadial warming events recorded in the Cariaco Basin sediments *(28)* were synchronous with D-O events observed in the Greenland GICC05 ice core chronology *(18, 19)* (Fig S3), and therefore representative of the wider Northern Hemisphere, we performed a χ^2 test on the age estimates. For Greenland Interstadials 13-15, only the timing of the onset could be used due to their uncertain duration *(16)*. For the Cariaco Basin, the transition was taken as the mid-point depth between the associated maximum and minimum values of 550 nm reflectance values, representing a northward migration of the ITCZ *(28)*; the mean calendar age and 1σ was estimated from the interpolated depth *(28, 33)*. The interpolated calendar ages were compared to the estimates of the same events using the GICC05 chronology where the maximum counting error approximates 2σ *(18, 19)*. The maximum counting error was halved to derive an estimate of 1σ. Ages associated with each event were then compared using the *C_Combine* function in the chronological software OxCal 4.1 *(34, 45, 51)*.

All interstadial events (apart from NEA-GS3b) *(42)* could be clearly identified in both the Cariaco Basin and Greenland records, and were within dating errors. It is important to note that the D-O tie-point approach does not assume the low-latitude response to be instantaneous. All that is required is the change in the tropics was within the age uncertainty of the chronological frameworks of GICC05 and Cariaco Basin-Hulu Cave (between 93 and 1196 years at 1σ; Table S3*)*. Crucially, the timing of the interstadials were found to be statistically indistinguishable (Table S3 and Fig. S4), indicating little, if any, stratigraphic lag with high latitudes *(18,19)*. This is consistent with a reduction in the latitudinal temperature gradient and a relatively rapid hemispheric-wide atmospheric response (*52*) as observed previously (*26-31*). Support for this conclusion is the close correspondence between abrupt increases in atmospheric methane (CH_4) and interstadial warming as preserved in Greenland as peaks in δ^{18}O; CH_4 emissions and changes in Cariaco

Basin (Hulu Cave) are closely linked to tropical hydrology *(24)*, implying any temporal lag between the high and low latitudes are years to decades rather than centuries. This important finding allows us to combine the estimates for the onset of the interstadials from both records to generate precise age constraints for the Northern Hemisphere (Table S3). The Greenland $\delta^{18}O$ record was therefore transferred onto the revised Cariaco-Greenland chronology using the Linage function in AnalySeries 2.0 *(53)*, and replotted (Table S4, Fig. 1). The precise duration of interstadial events were provided from the Greenland ice core *(16)*, thereby establishing the timing and duration of intervening stadial events. It is important to note that the original Greenland $\delta^{18}O$ isotopic data remain unchanged, with only the timescale rescaled through the combination of the Cariaco and Greenland chronologies. For robust testing of calibrated megafaunal ages against climate we therefore used the Cariaco Basin radiocarbon dataset for comparison with two detailed climate records: the existing GICC05 ice core chronology *(18, 19)* and our new combined Cariaco-Greenland record.

Randomization tests for overlap with climatic events

A randomization approach was used to test the null hypothesis that the major megafaunal transitions (extinctions and invasions) and their associated uncertainty were distributed randomly in time relative to the temporal distribution of the observed regional warming and cooling events recorded in the GICC05 and Cariaco-Greenland timescales (Table S3). This approach was necessary as the precision on individual radiocarbon dates (and resulting GRIWM estimates) are sufficiently large for dates older than 30 kyr to make it impractical to test the correlation with an individual interstadial or stadial. Testing the correlation between all the events and the climate record circumvents this issue.

For each data series, we used both the 95% confidence interval of the GRIWM estimate of the terminal age, and the error range (2σ) on the *Phase*-calibrated terminal AMS date.
We first tested the hypothesis that extinctions and invasions were distributed randomly relative to the 'warm' events (interstadials) by randomizing the temporal placement of actual interstadial durations relative to the megafaunal transitions on the GICC05 timescale. We estimated how often the observed genetic transition events overlapped the time-randomized interstadials with 10,000 iterations, and then compared this sum to the observed overlap. The number of randomized overlaps equal to or exceeding the number of observed overlaps divided by the number of iterations is the probability that the null hypothesis is true. We repeated this randomization procedure with the 'cold' stadial events to test the hypothesis that the observed extinction/invasion pattern was randomly distributed in time relative to cold events.

We excluded the *Bison priscus* (invasion) and *Panthera leo* Beringia (invasion) from all simulations as the error margins were extremely large, and covered multiple stadial and interstadial events (see above). Wide CIs: We explored the impact of excluding/including the remaining group of events with wider confidence intervals (Fig. S1) from the simulations, and found that in general, exclusion resulted in fewer iterations where the observed result could be generated randomly. For the GRIWM analyses, wide-CI events were: *Ovibos*, Wrangel rhino, Beringian cave lion, *Bison priscus*, *Bison x* (invasion), mammoth clade III and mammoth clade I (invasion). For the terminal phase-calibrated AMS ages, the wide-CI events were: *Ovibos* and *Equus francisci*.

Constraints: Where the temporal ranges of two data series describing a replacement event (i.e., cave lion, bison, mammoth clades I/III) overlapped, we explored the effect of constraining the uncertainty of the event (Fig. S5). Simulations were performed with and without constraints applied.

We observed a strong, non-random correlation between extinction/invasion events and interstadials, but not stadials, in both the GICC05 and Cariaco-Greenland chronologies (Table 1). To explore the impact of different parameters, we performed simulations with the following additional variables: removing the potential effect of human-associated terminal Pleistocene events in the New World or Eurasia by leaving just post-LGM events from the NW, Eurasia, or neither (Pre-LGM); using all observed events or just extinctions alone (extinctions only); using a constrained range overlap to reduce error margins around an event where a rapid replacement by a congener or conspecific was observed (constrained range overlaps, Fig S5); with and without events with wide confidence intervals (wide-CI events).

There was a strong negative relationship between the number of episodes used in the particular combination of underlying selection criteria (Table 1) and the estimated probability of the null hypothesis being true (*p*) for both the GICC05 (Fig. 2) and Cariaco-Greenland chronologies (Fig. S6).

For GICC05, the overlap probability intervals shown on the y-axis of Fig. 2 are non-linear because they are a back transformation of the complementary log-log scale, $\log_{10}$-($\log_{10}$(1-*p*)); this was done to account for higher variances near the extremes (0, 1) of the probability range. There was more statistical support (i.e., higher information-theoretic evidence-ratio) for the linear decline model (negative slope: dashed lines) versus the null model (i.e., no effect of changing number of extinction/invasion events) describing the relationship between the *p* of random interstadial overlap and number of extinction/invasion events for Terminal AMS data (Fig. 2 panel a: linear decline model Akaike's information criterion [AIC] weight = 0.967; evidence ratio [*ER*] versus null model = 28.9; $r^2 = 0.29$) but not GRIWM (Fig. 2 panel c: linear decline model *w*AIC = 0.36; *ER* = 0.56; $r^2 = 0.05$). The *ER* is a relative measure of model fit, and can be read as the amount of information-theoretic support model *X* receives relative to model *Y*, e.g. if *ER*(X:Y) = 10 then model *X* has ten times more information-theoretic support than model *Y* based on the data. For the datasets considering extinction events only, the *ER* = 66.5 for Terminal AMS (Fig. 2 panel b) and 0.15 for GRIWM (Fig. 2 panel d). This demonstrates that the power of detecting a non-random interstadial overlap is partially contingent on the number of extinction/invasion events considered.
For the Cariaco-Greenland chronology (Fig. S6), the above relationship had an *ER* = 212.54; $r^2 = 0.40$ for Terminal AMS estimates and *ER* = 1.83; $r^2 = 0.18$ for GRIWM when extinctions and invasions were considered together. For simulations including extinction events only, the *ER* = 158.29 for Terminal AMS and 0.41 for GRIWM.

The power relationship with the number of events per simulation meant that we did not have sufficient power to test all possible selection-criteria combinations. For example, we could not test all hypotheses about the relative role of humans in the extinction or invasion episodes. When we excluded both New and Eurasian post-LGM events, where human involvement has been suggested, the remaining number of observations was insufficient to provide enough statistical power to test the relationships. However, we still found low *p* for simulations excluding either New World or Eurasia post-LGM events.

More of the tests that detected non-random overlaps with interstadial events involved datasets based on Terminal-AMS, rather than GRIWM, estimates. This trend is likely to reflect the wider confidence intervals associated with the GRIWM measures that increases the likelihood of random overlap with both interstadials and stadials, especially in the older events, decreasing the ability to detect specific associations. In addition, the GRIWM estimates might over-estimate the time required for demographic decline to local extinction if

the terminal phase of megafaunal population presence in an area collapses quickly – for example following rapid environmental change. In such situations the terminal AMS date might be a more appropriate measure.

There also appears to be a consistent trend within the datasets based on GRIWM estimates towards non-random overlaps when extinction events are considered alone, rather than combined datasets of both extinction and invasion events. This trend might reflect a stronger relationship between the interstadial events and extinctions, or could suggest that invasions are taking place under different climatic conditions. However, this could also reflect individual species-specific responses, or differing probabilities of accurately estimating the date of the last or first members of a species in an area depending on the underlying demographic patterns.

From an entirely statistical perspective, we expect that a non-random association of megafaunal transitions with stadials would not be detected, precisely because an association is detected with interstadials. Given that stadials and interstadials represent mutually exclusive states, the detection of a non-random association with interstadials means by definition that the transition events must be random with respect to stadials.

Younger Dryas (YD) stadial event and megafaunal transitions

The YD stadial preceding the Holocene warm period has often been hypothesized as a prime driver of extinctions *(3, 22)*. However, Figure 1 suggests the megafaunal transitions appear to be primarily distributed in the warm periods on either side of the YD, particularly the preceding Interstadial 1. To test this, we calculated the proportion of the confidence interval of each event that falls into either the Holocene, YD or Interstadial 1 on the Cariaco-Greenland chronology, where we standardized the duration of each event to equal that of the YD event. After standardizing the resultant percentages to sum to 100 %, we tested whether there was departure from the null hypothesis of equal overlap among the three events using a generalized linear model with 'event' as a binary explanatory factor. Compared to the null intercept-only model (i.e., equal overlap among the three climatic periods), there was evidence for a higher overlap in Interstadial 1 relative to the other events for both phase-calibrated terminal AMS estimates (information-theoretic evidence ratio [*ER*] = 6.3), and GRIWM estimates (*ER* = 1.1) (Fig. S7). Remarkably, this association towards interstadials is in spite of the presence of a radiocarbon plateau through the YD chronozone *(36)*, which would skew ages towards the middle of the stadial. This provides further support to our observation that the pattern of pre-LGM interstadials is linked to major megafaunal transitions, while stadials do not appear to have such a correlation.

Climatic and ecological implications

In addition to the well-known cluster of megafaunal transition events at the terminal Pleistocene, there also appears to be a noticeable concentration around IS5 and 6/7, towards the end of the series of prominent Bond Cycles observable from at least 60 kyr (Fig. 1). This appears to be well before the cold downturn leading to the LGM (which occurs around 26 kyr) that has previously been advocated as a causative factor *(4, 41)*. There appears to be no evidence for the role of a putative bolide impact at 12.9 kyr in the terminal Pleistocene megafaunal extinctions *(54)* as there is little relationship between this date and the megafaunal transitions. Furthermore, multiple taxa appear to survive this event.

To characterize the rate of environmental change as inferred from the $\delta^{18}O$ time series of the new combined Cariaco-Greenland record, we also calculated a 500-year running mean of the coefficient of variation (CV) of the 20-year $\delta^{18}O$ values (the CV of all the values within a 500-year window was calculated as a running mean). This plot demonstrated peak values of change during the onset of interstadials (Fig. S8), and to a lesser extent the end of interstadials, confirming the likely rapid impacts of these events on Holarctic environments.

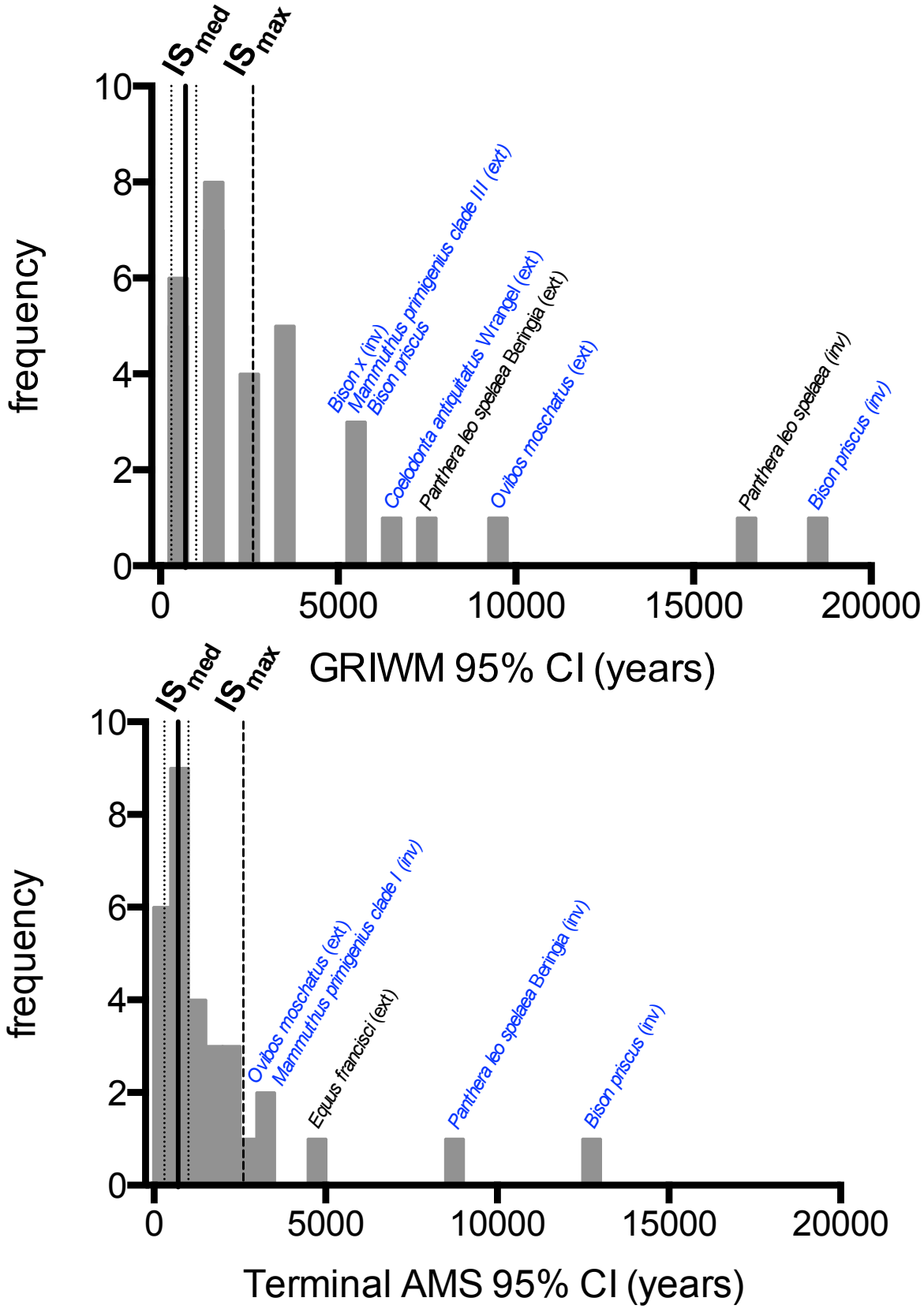
IS med
IS max
frequency
10
8
6
4
2
0
0
5000
10000
15000
20000
GRIWM 95% CI (years)
Bison x (inv)
Mammuthus primigenius clade III (ext)
Bison priscus
Coelodonta antiquitatus Wrangel (ext)
Panthera leo spelaea Beringia (ext)
Ovibos moschatus (ext)
Panthera leo spelaea (inv)
Bison priscus (inv)
IS med
IS max
frequency
10
8
6
4
2
0
0
5000
10000
15000
20000
Terminal AMS 95% CI (years)
Ovibos moschatus (ext)
Mammuthus primigenius clade I (inv)
Equus francisci (ext)
Panthera leo spelaea Beringia (inv)
Bison priscus (inv)

Fig. S1.

Distribution of the width of 95% confidence intervals for GRIWM (top) and terminal *Phase*-calibrated AMS estimates (Terminal AMS – bottom) calculated for different taxa and events (blue for Old World, and black for New World). Those intervals spanning more than 5,000 years (which tended to be for the oldest series) were clear outliers, and were classified as 'wide' confidence intervals and not used in the randomization tests because they cover multiple interstadial or stadial events, undermining the power of the tests.

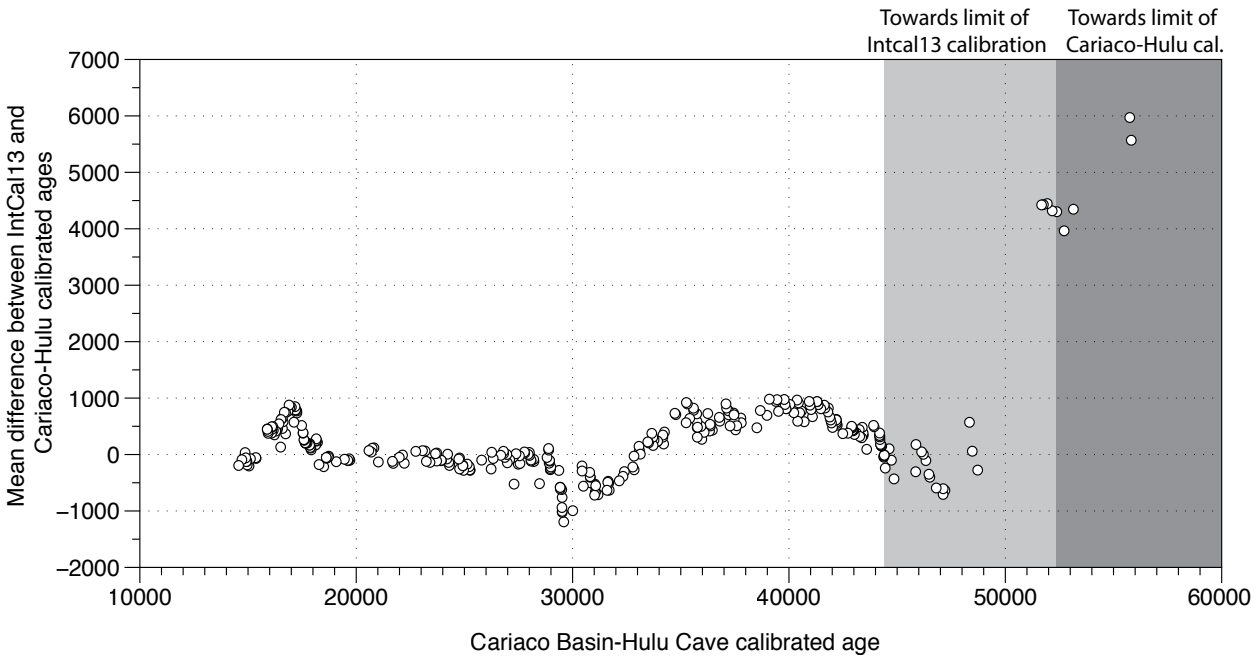

Fig. S2

Comparison of mean Cariaco Basin and IntCal13 calibrated ages obtained from 355 radiocarbon dated Eurasian mammoths >12,500 ^{14}C years. The calendar-age timescale for Cariaco Basin record has been generated by correlation with the Hulu Cave record.

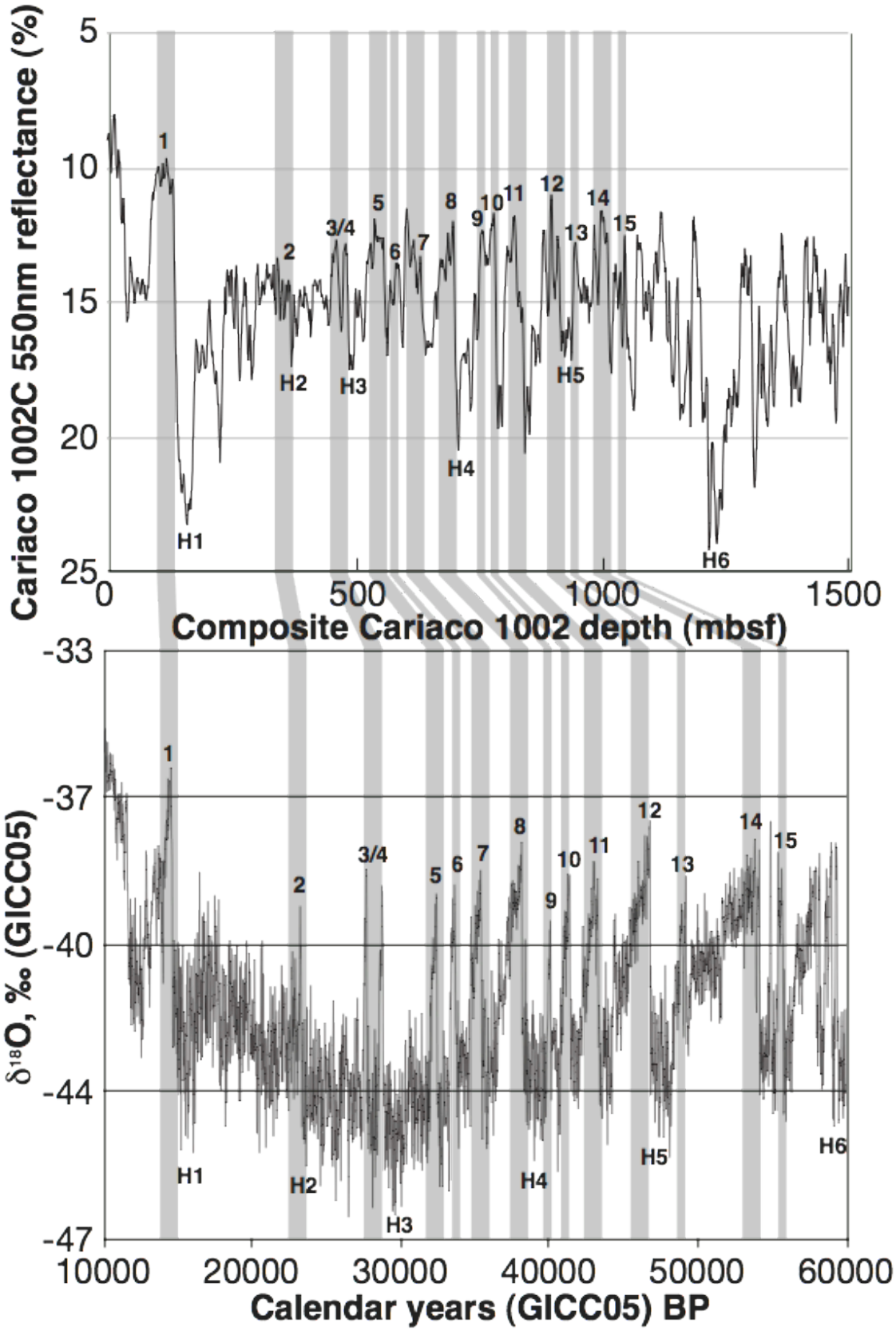
Cariaco 1002C 550nm reflectance (%)
5
10
15
20
25
0
500
1000
1500
Composite Cariaco 1002 depth (mbsf)
1
2
3/4
5
6
7
8
9
10
11
12
13
14
15
H1
H2
H3
H4
H5
H6
δ18O, ‰ (GICC05)
-33
-37
-40
-44
-47
10000
20000
30000
40000
50000
60000
Calendar years (GICC05) BP

Fig. S3

Correlation of Cariaco Basin marine core (above) and Greenland ice core palaeoclimate (below) datasets over the past 60,000 years. Numbers in bold denote interstadial events as recognised in the Greenland ice core record; Heinrich events are given by a bold 'H' followed by a number. The transitions into the Cariaco Basin interstadials were taken as the mid-point depth between the associated maximum and minimum values of 550 nm reflectance values, representing a northward migration of the ITCZ *(28)*. The Greenland ice core $\delta^{18}O$ is plotted on the Greenland Ice Core Chronology 2005 - GICC05 *(18, 19)*; the timing and duration on the interstadials are from Wolff *et al. (16)*.

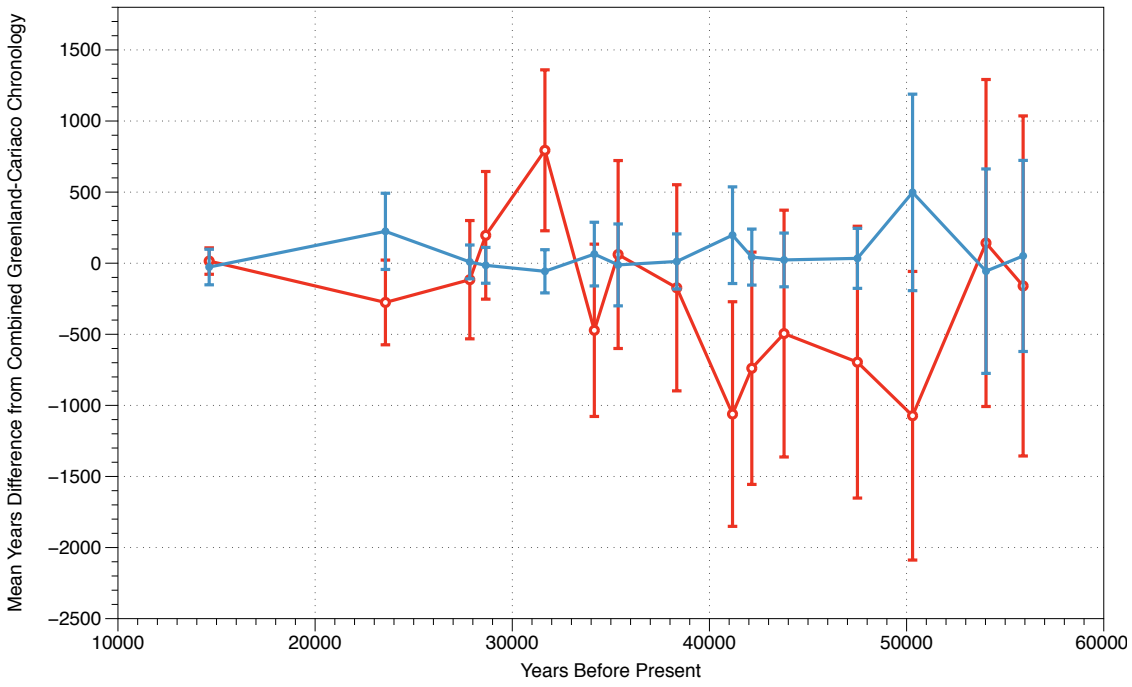

Fig. S4

Mean age difference between the newly developed combined Cariaco-Greenland chronology and onset of interstadials in Greenland (GICC05; red circles) *(18, 19)* and Cariaco Basin (on revised Hulu Cave timescale; blue circles) *(28, 33)*, data from Table S3.

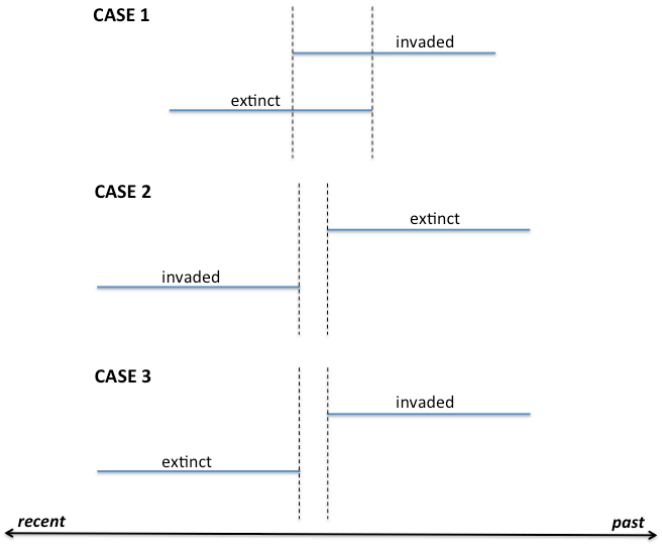

Fig. S5

Constraining events based on clade transitions. In Case 1, the overlap between the confidence intervals of the invasion and extinction events becomes the constrained interval for both events. In Cases 2 and 3, the temporal window between the estimated extinction and invasion event confidence intervals is used as the constrained event time.

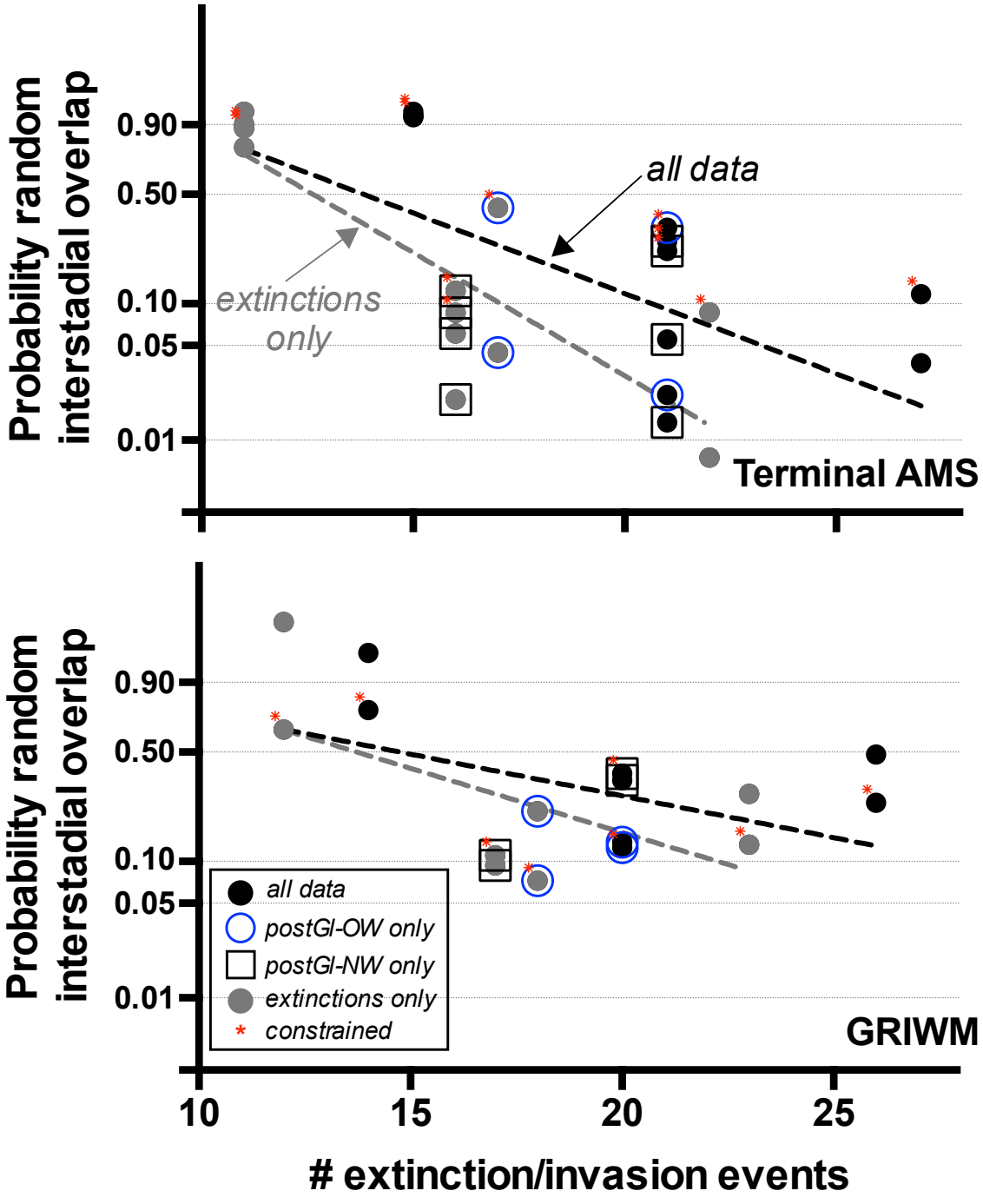

Fig. S6

A strong correlation is apparent between megafaunal transitions (extinctions/invasion events) and interstadials in the combined Cariaco-Greenland chronology, similar to the relationship obtained using the standard GICC05 chronology (Fig. 2). The probability of generating the observed overlaps of events with

interstadials randomly (p) is inversely related to the number of events measured for both GRIWM (black line) and terminal calibrated AMS events (red line), while the probabilities of random association for stadials were all > 0.60 (Table 1). The plotted data are from simulations excluding events with wide confidence intervals (above), as inclusion of the latter nearly always resulted in a greater chance of overlap being random (i.e., higher p). There was more statistical support (higher information-theoretic evidence-ratio) for the linear decline model (negative slope: dashed lines) versus the null model (i.e., no effect of changing number of extinction/invasion events) describing the relationship between the p of random interstadial overlap and number of extinction/invasion events for Terminal AMS data (linear decline model Akaike's information criterion [AIC] weight = 0.995; evidence ratio [ER] versus null model = 212.5; $r^2 = 0.40$) and GRIWM (linear decline model AIC weight = 0.65; $ER = 1.83$; $r^2 = 0.18$). This demonstrates that the power of detecting a non-random interstadial overlap is partially contingent on the number of extinction/invasion events being analysed.

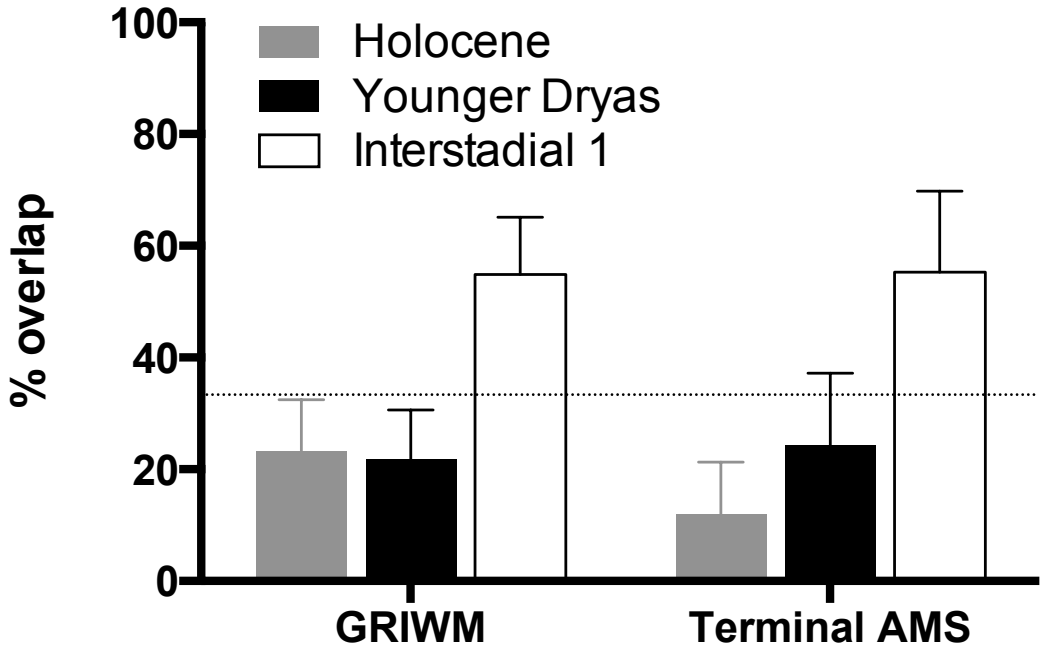

Fig. S7

Mean (+ SE) percentage overlap of 11 species' GRIWM and calibrated terminal AMS (Terminal AMS) extinction 95% confidence intervals with the Holocene, Younger Dryas and Interstadial IS1 periods (see Fig. 1). In this test, the Holocene and IS1 were standardised to be the same duration as the Younger Dryas (subsequent overlap percentages per time series standardised to sum to 100 %) using the Cariaco-Greenland chronology. The null hypothesis of equal distribution (33.3 %) is shown as a horizontal dotted line. For both GRIWM and phase-calibrated terminal AMS, events fell non-randomly more often into IS1 and less frequently than expected by chance in the YD and Holocene.

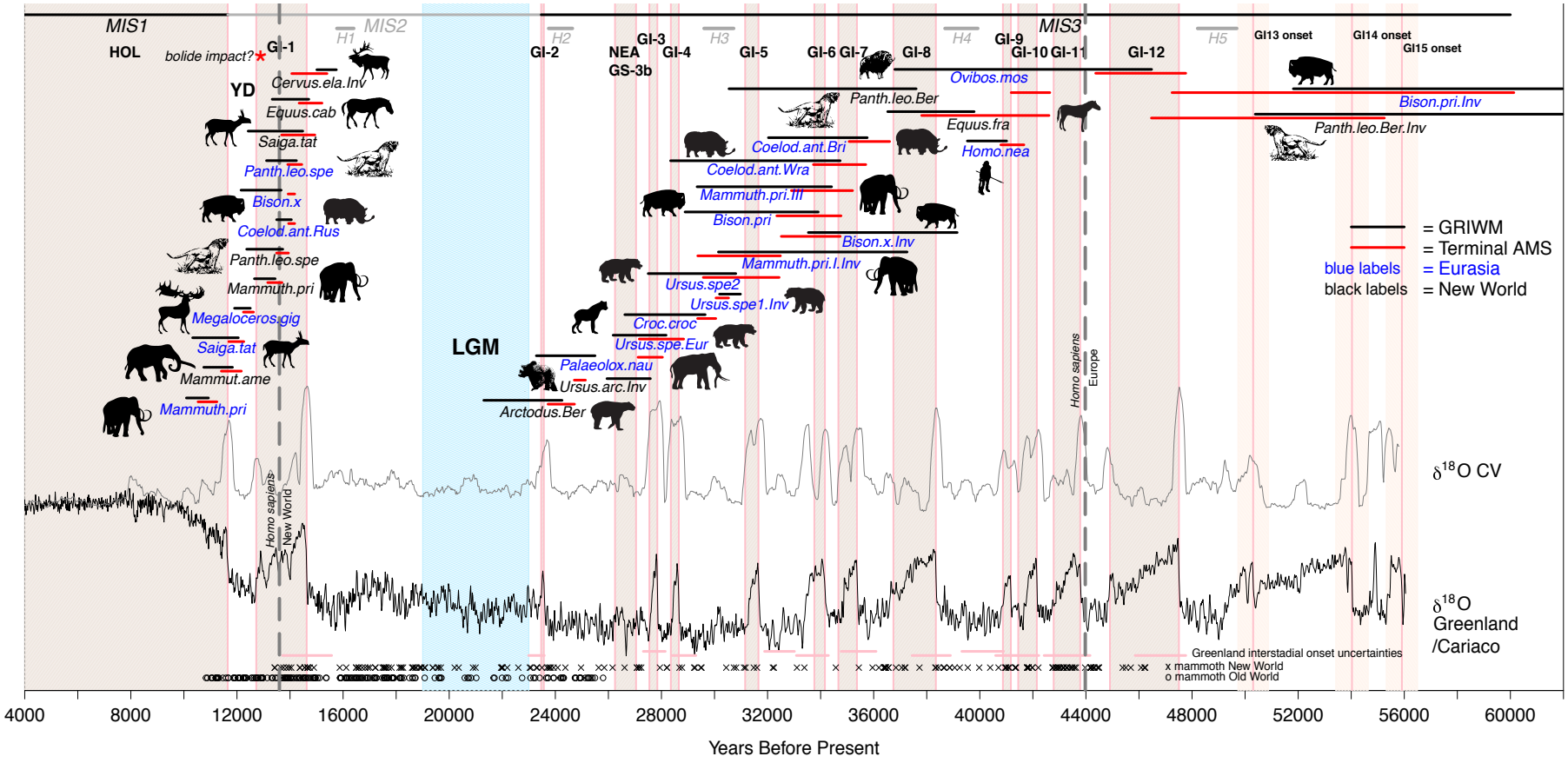

Fig. S8

The recalibrated Greenland record (black line) calculated from the combined Cariaco-Greenland chronology (Table S4) was used to generate a 500-year running window calculating the coefficient of variation ($\delta^{18}O$ CV) to highlight periods of likely rapid environmental change, highlighting the impacts at the onset and ending of interstadials, and relationships to the megafaunal transition events. The timing of interstadials is shown according to the recalibrated Greenland record, with the pink bars below representing the error margins (1 sd) for the estimated onset of GI events in the GICC05 chronology.

Table S2.

Summary of 31 megafaunal time series compiled for climate-event randomisations. For each species, the youngest and oldest uncalibrated terminal AMS radiocarbon dates in the series are shown (with one standard deviation), and the number of dates (*n*) in the series used to calculate the OxCal *Phase*-calibrated first or final dates, and the GRIWM extinction or invasion 95 % confidence interval. Full details of individual dates, data series and results are presented in Table S1. The youngest dates are relevant for extinction events, the oldest dates for invasions.

Genus	species	type	loc	nature of event	Youngest AMS in series (SD)	Oldest AMS in series (SD)	*n*	Young. AMS phase calibrated	Old. AMS phase calibrated (SD)	GRIWM range	Event record
Arctodus	*simus*	ext	NW	Last occurrence of species in eastern Beringia (Alaska/Yukon).	20210 (110)	44240 (930)	15	24224 (251)	Not relevant	21301 – 24255	Fossil
Bison	*priscus*	ext	OW	Last occurrence of species of B. priscus in western Europe towards end of MIS3.	29060 (140)	51800 (1300)	11	33558 (606)	Not relevant	28887 – 33911	DNA
Bison	*priscus*	inv	OW	First occurrence of B. priscus in w. Europe in MIS 3. Not used in randomisations, large error margins due to a	29060 (140)	51800 (1300)	11	Not relevant	53688 (3222)	51816 – 70106	DNA
Bison (X)	*n. sp.*	ext	OW	New species (detected genetically). Extinction in Europe.	12160 (40)	29230 (150)	12	14053 (63)	Not relevant	12151 – 13668	DNA
Bison (X)	*n. sp.*	inv	OW	First occurrence of new species in Europe after disappearance in late MIS4	12160 (40)	29230 (150)	11	Not relevant	33628 (557)	33535 – 39149	DNA
Cervus	*elaphus*	inv	NW	First occurrence in eastern Beringia (Alaska/Yukon).	10120 (110)	12770 (240)	58	Not relevant	14729 (333)	15009 – 15749	Fossil
Coelodonta	*antiquitatis*	ext	OW	Last occurrence of species in Britain	31140 (170)	55571 (3363)	24	35837 (383)	Not relevant	32029 – 35759	Fossil
Coelodonta	*antiquitatis*	ext	OW	Last occurrence of species in Russia/Europe	12155 (37)	25040 (120)	85	14061 (59)	Not relevant	13493 – 14053	Fossil
Coelodonta	*antiquitatis*	ext	OW	Last occurrence of species on Wrangel Island	29800 (340)	37780 (310)	7	34715 (495)	Not relevant	28342 – 34738	Fossil
Crocuta	*spelaea*	ext	OW	Last occurrence of species in Europe.	26120 (330)	39900 (700)	45	29705 (173)	Not relevant	26616 – 29650	Fossil
Equus	*caballus*	ext	NW	Last occurrence of species in eastern Beringia (Alaska/Yukon).	12482 (80)	16700 (220)	24	14773 (217)	Not relevant	13326 – 14710	Fossil
Equus	*francisci*	ext	NW	Last occurrence of species in eastern Beringia (Alaska/Yukon).	31400 (1200)	40800 (3900)	19	40209 (1201)	Not relevant	36526 – 39788	Fossil
Homo	*neanderthalensis*	ext	OW	Last occurrence in European record.	35500 (216)	52700 (2000)	150	41227 (219)	Not relevant	39528 –41013	Fossil
Mammut	*americanum*	ext	NW	Last occurrence of species in North America.	10055 (40)	12350 (65)	20	11788 (190)	Not relevant	10746 – 11834	Fossil
Mammuthus	*primigenius*	ext	NW	Last occurrence of species in eastern Beringia (Alaska/Yukon).	11500 (160)	14830 (180)	32	13428 (136)	Not relevant	12656 – 13422	Fossil
Mammuthus	*primigenius*	ext	OW	Last occurrence of species in Europe/western Beringia (excl. Wrangel Island etc).	9470 (40)	12000 (130)	42	10888 (179)	Not relevant	10092 – 10927	Fossil
Mammuthus	*primigenius*	ext	OW	Last occurrence of clade III in Europe	29030 (400)	47500 (2300)	17	34050 (578)	Not relevant	29341 - 34415	DNA
Mammuthus	*primigenius*	inv	OW	Invasion of clade I in Europe	14095 (55)	27630 (140)	8	Not relevant	30926 (780)	30145 - 37260	DNA
Megaloceros	*giganteus*	ext	OW	Last occurrence of species in western Europe (not Urals).	10257 (75)	12850 (250)	43	12433 (96)	Not relevant	11906 - 12506	Fossil
Ovibos	*moschatus*	ext	OW	Last occurrence of clade 1, in Beringia.	42550 (450)	49700 (3400)	4	46065 (850)	Not relevant	36793 – 46478	Fossil
Palaeoloxodon	*naumanni*	ext	OW	Last occurrence of species in Japan.	23600 (130)	34010 (180)	9	27577 (231)	Not relevant	23282 – 25499	Fossil
Panthera	*leo spelaea*	ext	OW	Last member of pre-bottleneck clade (non A-E) in Europe/Beringia.	36550 (290)	55700 (3000)	7	41911 (365)	Not relevant	30544 – 37603	DNA
Panthera	*leo spelaea*	ext	NW	Last occurrence of species in eastern Beringia (Alaska/Yukon).	11925 (70)	53900 (2300)	20	13717 (113)	Not relevant	12364 - 13728	Fossil
Panthera	*leo spelaea*	ext	OW	Final extinction of species in Europe/Beringia.	12248 (66)	17915 (70)	15	14179 (134)	Not relevant	13111 – 14244	Fossil
Panthera	*leo spelaea*	inv	OW	First occurrence of bottleneck clade (A-E) in Eur./Bering. Not used in randomisations - age and quality of date	11925 (70)	49900 (1500)	18	Not relevant	50859 (2196)	50381 – 66646	DNA
Saiga	*tartarica*	ext	NW	Last occurrence of species in eastern Beringia (Alaska/Yukon).	12220 (130)	14920 (160)	7	14309 (314)	Not relevant	12420 – 14482	Fossil
Saiga	*tartarica*	ext	OW	Last occurrence of clade 2 (north of Urals).	10250 (55)	15030 (80)	6	11976 (142)	Not relevant	10327 – 12053	DNA
Ursus	*arctos*	inv	NW	First occurrence of clade 3b in eastern Beringia.	9335 (75)	20820 (120)	17	Not relevant	24926 (106)	25944 – 27585	DNA
Ursus	*spelaeus*	ext	OW	Last occurrence of clade 2 in Ach Valley, Germany.	27840 (190)	38010 (520)	13	31006 (716)	Not relevant	27498 – 30804	DNA
Ursus	*spelaeus*	ext	OW	Last occurrence of species in Europe.	23780 (120)	29810 (270)	29	28001 (419)	Not relevant	26177 – 28178	Fossil
Ursus	*spelaeus*	inv	OW	First occurrence of clade 1 in Ach Valley, Germany.	25560 (130)	27870 (190)	7	Not relevant	30293 (120)	30187 – 30981	DNA

Table S3.

Summary of ages for interstadial and Holocene ('Hol') warming over the past 56,000 years using the Greenland ice core GICC05 and Cariaco Basin marine sedimentary records, along with the combined mean age (at 1σ) used to construct the new chronology. *t* values from χ^2 test of variance for combined ages derived from Oxcal *(34)*.

Interstadial	Greenland onset, cal. BP[1]	±1σ	Cariaco onset, cal. BP[2]	±1σ	*t* (5% 3.8)	Combined mean age, cal. BP (onset of Interstadial)	±1 σ	Offset from Greenland (% change in error)	Offset from Cariaco (% change in error)	Termination of Interstadial[1]
Hol	11,653	50				*11,653*	*50*			
GI-1	14,642	93	14,600	125	0.1	14,627	76	15 (18.3)	-27 (39.2)	12,727
GI-2	23,290	298	23,790	268	1.6	23,566	201	-276 (32.6)	224 (25.0)	23,466
NEA-GS-3b[c]			27,042	205		*27,042*	*205*			26,250
GI-3	27,730	416	27,855	119	0.1	27,846	116	-116 (72.1)	9 (2.5)	27,546
GI-4	28,850	449	28,639	126	0.2	28,654	123	196 (72.6)	-15 (2.4)	28,354
GI-5	32,450	566	31,599	152	2.1	31,656	148	794 (73.9)	-57 (2.6)	31,156
GI-6	33,690	606	34,226	224	0.7	34,162	213	-472 (64.9)	64 (4.9)	33,762
GI-7	35,430	661	35,357	288	<0.1	35,369	266	61 (59.8)	-12 (7.6)	34,669
GI-8	38,170	725	38,355	194	0.1	38,343	189	-173 (73.9)	12 (2.6)	36,743
GI-9	40,110	790	41,368	340	2.1	41,171	314	-1,061 (60.3)	197 (7.6)	40,871
GI-10	41,410	817	42,192	197	0.9	42,149	193	-739 (76.4)	43 (2.0)	41,449

Interstadial	Greenland onset, cal. BP[1]	±1σ	Cariaco onset, cal. BP[2]	±1σ	*t* (5% 3.8)	Combined mean age, cal. BP (onset of Interstadial)	±1 σ	Offset from Greenland (% change in error)	Offset from Cariaco (% change in error)	Termination of Interstadial[1]
GI-11	43,290	868	43,808	189	0.3	43,785	186	-495 (78.6)	23 (1.6)	42,785
GI-12	46,810	956	47,540	211	0.6	47,506	208	-696 (78.2)	34 (1.4)	44,906
GI-13	49,230	1,015	50,801	691	1.6	50,303	573	-1,073 (43.5)	498 (17.1)	
GI-14	54,170	1,150	53,972	719	<0.1	54,028	610	142 (47.0)	-56 (15.2)	
GI-15	55,750	1,196	55,961	672	<0.1	55,910	587	-160 (50.9)	51 (12.6)	

[1] Derived from Greenland *(16)*

[2] Derived from Cariaco Basin *(28, 33)*

[3] Identified in North Atlantic records *(42)* and described as a ~800 year duration event; not observed in Greenland.

Additional Data Table S1 (separate file)

Details of the AMS radiocarbon series for each taxon used in the analyses, including references. The data are calibrated using IntCal13/Cariaco calibrations, the *Phase* function of Oxcal *(34, 45)*, and the GRIWM estimates. GRIWM estimates of the range for the actual extinction date of each taxon are presented in yellow as the lower and upper bounds, median value and standard deviation. The GRIWM data series are highlighted in green. Yellow highlighting is also used to indicate the calibrated terminal age, 1 standard deviation, and the absolute time range at 2 standard deviations. The boundary ages (End 1 and Start 1) describe the modelled boundaries of the distribution of the data series calculated by the *Phase* function in Oxcal *(34, 45)*, and are not used, in preference for the more conservative GRIWM approach. Calendar ages are expressed relative to C.E. 1950 (Before Present or B.P.).

Additional Data Table S4 (separate file)

The bi-decadally resolved Greenland ice core $\delta^{18}O$ record (relative to Before Present; B.P.), developed by combining the Cariaco Basin (3.14c. Hulu Cave) and GICC05 chronologies *(18, 19, 28, 33)*.